INSTITUTE OF PHYSICS PUBLISHING JOURNAL OF PHYSICS: CONDENSED MATTER

J. Phys.: Condens. Matter **16** (2004) S4231–S4242 PII: S0953-8984(04)81162-7

Confocal scanning laser microscopy on fluid–fluid demixing colloid–polymer mixtures

D G A L Aarts and H N W Lekkerkerker

Van 't Hoff Laboratory, Debye Research Institute, University of Utrecht, Padualaan 8, 3584 CH Utrecht, The Netherlands

E-mail: d.g.a.l.aarts@chem.uu.nl

Received 26 April 2004
Published 10 September 2004
Online at stacks.iop.org/JPhysCM/16/S4231
doi:10.1088/0953-8984/16/38/035

Abstract

We study gas–liquid phase separating colloid–polymer mixtures using a horizontally placed confocal scanning laser microscope. The phase separation proceeds via spinodal decomposition; first images immediately show sharp interfaces, which is explained in terms of the colloid diffusion time. The diffusion in both the liquid and gas phase is measured in a real space fluorescence recovery after a photo-bleaching experiment. The coarsening rate of the characteristic length in the system can be understood in terms of the capillary velocity. We observe that the spinodal structure collapses due to gravity at a typical size of the order of the capillary length, which is obtained from the static gas–liquid profile near a single wall and is accurately described by the interplay between hydrostatic and Laplace pressure. The present technique allows for precise contact angle measurements and the system shows complete wetting for all statepoints measured. Finally, we study the possibility of capillary condensation in colloid–polymer mixtures and show first indicative experimental results. The observed Kelvin length is surprisingly large, possibly because the system is not yet in complete equilibrium.

(Some figures in this article are in colour only in the electronic version)

1. Introduction

Adding non-adsorbing polymer to a colloidal suspension may induce a fluid–fluid demixing transition that is widely accepted to be the mesoscopic analogue of the liquid–gas phase transition in molecular systems [1]. The coexisting phases are a colloidal liquid (rich in colloid and poor in polymer) and a colloidal gas (poor in colloid and rich in polymer). These mixtures have several attractive features and here we show the possibilities and advantages of studying such mixtures with confocal scanning laser microscopy (CSLM).

The main advantage of confocal microscopy over transmission light microscopy is that a thin slice of the system is imaged with a thickness $\sim$0.6 μm [2] (for an objective with a numerical aperture of 1.4). Hence, shadow and reflection effects are minimal and even when focusing deep inside the sample images are not blurred. Thus, this technique allows high resolution 3D imaging and can for example be used to track the coordinates of thousands of colloids in 3D [3] with a diameter of $\geqslant$1 μm, but here we will use it on a super-particle level, which brings advantages of its own.

One of the attractive features of colloid–polymer mixtures is that the colloids can be chemically engineered to make them for example fluorescent. In this case it is possible to use confocal scanning laser microscopy. Furthermore, for colloid–polymer mixtures the interactions are tunable [4–6]; a polymer coil is entropically excluded from a region around a (colloidal) surface, the depletion zone. Its thickness depends on the size and hence the molecular mass of the polymer. If two such depletion zones overlap there is an osmotic imbalance, whose strength depends on the polymer concentration, pushing the particles together. In addition, the colloid–polymer size ratio sets the general phase behaviour. Furthermore, the buoyant mass of the particles can be tuned such that the influence of gravity can be explored [7, 8]. Finally, it is known from experiment [9–13] and theory [14–18] that in such systems the interfacial tension, γ, scales far away from the critical point as

$$\gamma \propto k_{\mathrm{B}}T/\sigma_{\mathrm{c}}^2, \tag{1}$$

with $k_{\mathrm{B}}T$ the thermal energy and σ_{c} the colloidal particle diameter. For particles of $\sigma_{\mathrm{c}} \sim 50$ nm, γ becomes of the order of μN m^{-1}. This has several consequences. The interface dynamics is up to very long length- and timescales simply described by Stokes flow as explained in detail in [12]. The corresponding interface velocity, i.e. the capillary velocity v_{cap}, equals

$$v_{\mathrm{cap}} = \frac{\gamma}{\eta} \tag{2}$$

with η the viscosity. It becomes of the order of tens of μm s^{-1}, which will be exploited in section 3. The capillary length l_{cap} defined as

$$l_{\mathrm{cap}} = \sqrt{\frac{\gamma}{\Delta\rho g}}, \tag{3}$$

with $\Delta\rho$ the mass density difference between gas and liquid phase and g earth's constant of acceleration, becomes of the order of tens of micrometres instead of several millimetres as in molecular fluids, and this will be studied in section 4. An interesting question is to what level a macroscopic description of the interface properties still holds on small lengths with large 'atoms'. If two walls are brought into close contact a gaseous phase will condense when the typical wall–wall separation is twice the Kelvin length l_{K}, which again is set by the interfacial tension:

$$l_{\mathrm{K}} = \frac{\gamma}{\Delta\mu\Delta n} \tag{4}$$

with $\Delta\mu$ the chemical potential difference between coexistence and undersaturation and with Δn the number density difference between the gas and liquid phases. This equation holds for one-component systems and becomes slightly modified for two-component systems. A theoretical framework and first experimental results of this phenomenon will be shown in section 5. Finally, we conclude our main findings in section 6.

2. Experimental system and technique

We prepared fluorescent poly(methylmethacrylate) (PMMA) colloidal spheres following the method of Bosma *et al* [19] slightly modified by using *cis/trans* decalin (Merck, for

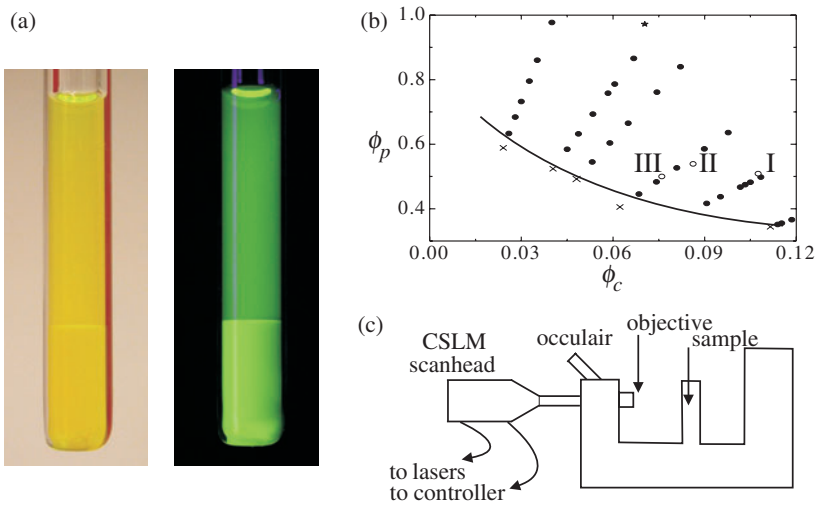

Figure 1. (a) Photographs of a phase separated mixture of fluorescently labelled PMMA colloids and polystyrene polymer in decalin. The left image was taken under normal light, the right one under UV light. The very sharp interface can be clearly seen. (b) Phase diagram in (ϕ_p, ϕ_c)-representation. Indicated are points where gas–liquid phase separation occurs (open and filled circles), statepoints where the system gelled (stars), and statepoints in the one-phase region (crosses). The line is an estimate of the binodal and is drawn to guide the eye. State points I, II and III are indicated (open circles). (c) Schematic CSLM setup.

synthesis) as reaction solvent. The (dynamic light scattering) radius R_c was 25 nm and the polydispersity was less than 10%, estimated from scanning electron microscopy images. As polymer, commercially available polystyrene (Fluka) was used with a molecular weight $M_w = 233$ kg mol^{-1} ($M_w/M_n = 1.06$, with M_n the number average molecular weight) and a radius of gyration R_g of $\sim$14 nm (calculated from data in the literature [20]). Both species were dissolved in decalin and since all densities were known, mass fractions could be directly converted to volume fractions of colloids, $\phi_c = \frac{4}{3}\pi R_c^3 n_c$, and of polymers, $\phi_p = \frac{4}{3}\pi R_g^3 n_p$, where n_c and n_p are the number densities of colloids and polymers, respectively. Samples were prepared by mixing colloid- and polymer-stock dispersions and diluting with decalin. At high polymer concentrations it took a few hours before the system phase separated completely, at intermediate concentrations about 15 min and very close to the binodal again up to hours. The resulting interfaces were very sharp, as can be seen in figure 1(a). In principle, the size ratio $q = R_g/R_c = 0.56$ allows for the observation of gas, liquid and crystal phases [21], but only gas–liquid phase coexistence was observed; see figure 1(b) for the phase diagram. Fluid–crystal coexistence was possibly suppressed by the polydispersity of the spheres, as is often the case in systems with small spheres, and the system gelled instead of displaying a crystal phase at relatively high polymer concentrations. To study the colloid–polymer mixtures we used the following setup, schematically shown in figure 1(c). A confocal scanning laser head (Nikon C1) was mounted on a horizontally placed light microscope (Nikon Eclipse E400). Large glass cuvettes (of volume $\sim$1 cm^3) with extra thin cover glass walls (0.17 mm thick) were fabricated in our laboratory. The setup allows for monitoring using the CSLM as well as the transmission light microscope.

3. Phase separation kinetics and morphology

In this section we show the results for bulk behaviour, i.e. behaviour without the influence of walls, and focus on the phase separation morphology and kinetics. The microscope records

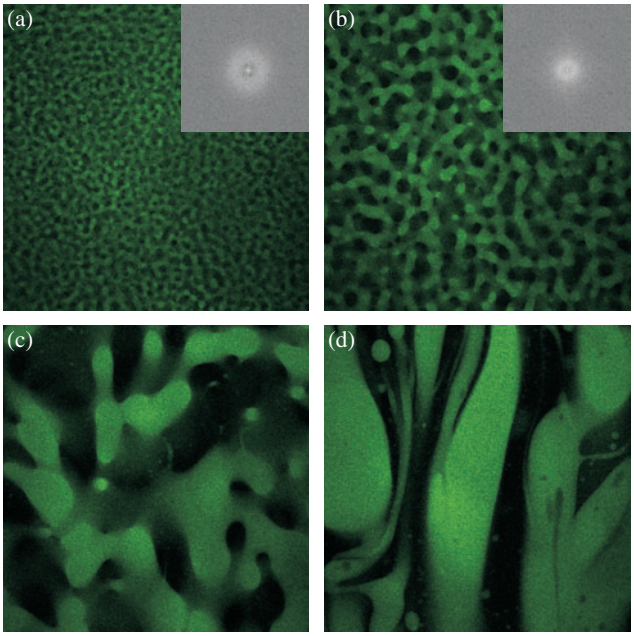

Figure 2. (a)–(d) CSLM images ($700 \times 700\ \mu m^2$) of a phase separating colloid–polymer mixture for statepoint I. Directly after homogenization a spinodal structure is observed ((a), $t = 6$ s), which coarsens in time ((b), $t = 15$ s) until the structure collapses and gravity driven flow kicks in ((c), $t = 50$ s) leading to lane-like structures ((d), $t = 102$ s). The insets in (a) and (b) are the discrete Fourier transforms.

the fluorescence of excited dye within the colloids, while the solvent and polymers are dark. Hence, the colloidal rich phase (liquid) appears bright, whereas the colloidal poor phase (gas) appears dark. Figure 2(a) displays a CSLM image about 6 s after homogenizing the sample. Since only a thin slice is imaged, it is immediately apparent what the underlying mechanism of phase separation is: either phase separation via nucleation and growth from the metastable region close to the binodal or via spinodal decomposition from the unstable region [22, 23]. Here, we see a typical spinodal pattern. The interfaces are already almost always sharp when the first image is taken, which is after about 4 s. This implies that the initial regime in spinodal decomposition in which the interfaces sharpen [24] is very short, as in the work of Verhaegh *et al* [25]. This is related to the colloid diffusion time and will be discussed below. Once the system has sharp interfaces the interfacial dynamics can be described up to large time- and lengthscales by Stokes flow, as explained in detail in [26, 12]. After about 15 s the system has substantially coarsened, see figure 2(b), showing dynamics in appearance very similar to simulations done by Pagonabarraga *et al* [27]. For example, coarsening occurs mainly through pinch-off events and not so much through coalescence.

The insets of figures 2(a) and (b) are discrete Fourier transforms of the CSLM images. By radially averaging the Fourier transform, see figure 3(a), one can easily obtain the typical size in the system. Although we perform a Fourier transform on a 2D image, Guenon *et al* [28] showed that the resulting radially averaged 'structure factor' agrees remarkably well with results from light scattering experiments, where the interfaces and not the domains are seen. Binder and Stauffer predicted that the structure factor, which we recognize here directly as $I(k, t)$, should scale dynamically as [29]

$$I(k, t) = k_{\max}^{-3} F(k/k_{\max}) \tag{5}$$

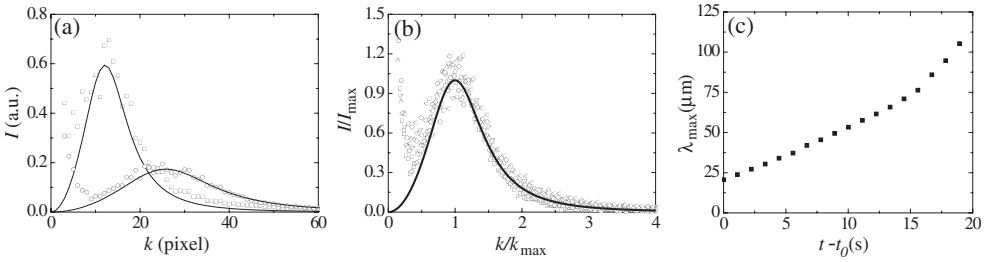

Figure 3. (a) Radial averages of the Fourier transforms of figure 2(a) (circles) and (b) (squares). One pixel corresponds to 2π over the image width. The curves follow from (6). The intensity increase at small k values stems from instrument properties (mainly the objective properties) and contains no relevant physical information. (b) Dynamical scaling of the structure factor as a function of $I/I_{\max}$ versus $k/k_{\max}$ for $t = 4$ s up to $t = 15$ s. The symbols correspond to five different data sets. The full curve is the prediction for off-critical demixing systems by Furukawa (6). From (a) the characteristic length can be found, which is plotted against time in (c) (minus the time between homogenization and the recording of the first image, $t_0 = 4$ s).

with $k_{\max}$ the time-dependent wavevector at the maximum intensity $I_{\max} \equiv I(k_{\max}, t)$ at time t and with F a universal scaling function. This scaling is not directly observed here, and it has been suggested [30–32] to divide the left-hand side of (5) by $\int I(k', t)k'^2\,\mathrm{d}k'$, which is explained in [25]. This integral is hard to perform in this real space experiment due to lack of statistics. By dividing $I(k, t)$ by $I_{\max}$ this problem is circumvented and $I(k, t)/I_{\max}$ collapses onto a single master curve as a function of $k/k_{\max}(t)$, shown in figure 3(b). The shape of the curve is quite well described by Furukawa's theory [33] for off-critical demixing systems,

$$I = I_{\max}\left(\frac{3(k/k_{\max})^2}{2 + (k/k_{\max})^6}\right), \tag{6}$$

as can be seen from the full curves in figures 3(a) and (b). The associated length L, found from the width of the image divided by $k_{\max}$ in pixels, is plotted as a function of time in figure 3(c), where at small times we see a linear increase of L with time as predicted by Siggia [34] for the late stages of spinodal decomposition with a continuous minority phase. For the present statepoint the gas phase occupies 58% and the liquid 42% of volume. The velocity associated with the initial coarsening is $\sim$3.4 μm s^{-1}, in good agreement with the estimate of Siggia [34], which gives a coarsening velocity of 0.1 times the capillary velocity (2).

After about 15 s the spinodal structure collapses under its own weight at a typical structure size of $\sim$75 μm. The subsequent hydrodynamic flow, see figures 2(c) and (d), can lead to the formation of distinct lanes of light phase moving up and heavy phase moving down [35]. In this case we do not get the formation of distinct lanes, but the coarsening occurs mainly in the direction of gravity and the Fourier transforms are flattened off. The typical size L at which the system collapses under its own weight equals [34]

$$L \sim \sqrt{\frac{\gamma}{\Delta\rho g}}. \tag{7}$$

Note that this size is exactly the capillary length l_{cap} (3) for which results are shown in section 4. There we see that the collapse occurs at about three times the capillary length, i.e. $\sim$75 μm. An intuitive derivation of (7) starts with the assumption that at the crossover to gravity driven coarsening the sedimentation velocity v_{s} becomes comparable to the capillary velocity v_{cap} [36]. The sedimentation velocity is given as

$$v_{\mathrm{s}} = \frac{m^* g}{f} \propto \frac{\Delta\rho L^3 g}{\eta L}, \tag{8}$$

with m^* the buoyant mass of the sedimenting object and f the friction. The buoyant mass is proportional to $\Delta\rho$ times the cube of the typical size L, whereas the friction is roughly the viscosity η times L. Equating these two velocities leads to (7). Recently, Wysocki and Löwen [37] indicated the relationship with the classical Rayleigh–Taylor instability. After this gravity driven flow the bulk interface is formed and becomes as sharp as shown in figure 1(a).

As noted above, the interfaces are already sharp in the first recorded images of phase separation. From linear Cahn–Hilliard theory [22, 23, 38, 39] we learn that in the early stage of phase separation the fastest growing wavevector is typically of the order of a few times the diameter of the colloid σ_c. Hence, after a time over which the colloids diffuse over for example $10\sigma_c$ one would expect to have sharp interfaces. It is difficult to measure diffusion coefficients during phase separation, but in a macroscopically phase separated system it is possible for example by bleaching a space cube in either the gas or liquid phase and following the recovery of intensity in time [40]. This is not only a way to measure the particle diffusion coefficient, but also is a way to test if the system is in equilibrium, i.e. to check for drift or convection.

We bleached a cuboid of (x, y) dimensions 40 μm^2 and of thickness $\sim$5 μm by illuminating the sample with a 405 nm laser. The dye incorporated in the particles was then easily destroyed. The subsequent recovery of intensity was monitored by using a 488 nm laser. Figure 4 shows the bleached cube at time $t = 0$ s (a) and after 28 s (b). We integrated the fluorescent intensities along the four (x, y) sides of the cube, corrected for the objective properties by dividing with the fluorescent intensity far away from the cube, and then normalized the intensity profiles. Averaging in the x direction of figure 4(a) gives the profiles along the y direction shown in figure 4(c). The other two profiles contain similar information. In [40] Simeonova and Kegel show the details of this technique and derive that the intensity profile along one side at time t can ideally be described by

$$I(x;t) = \frac{1}{2}\left(1 - \mathrm{erf}\left[\frac{x - x_0}{2\sqrt{Dt}}\right]\right), \tag{9}$$

with D the diffusion coefficient. In practice, broadening of the profile contained in the square-root term is also caused by the objective properties, and we therefore write $\sqrt{Dt + b} = \sqrt{C}$ in stead of $\sqrt{Dt}$ with b a constant. The full curves in figure 4(c) are the fits to (9) with x_0 and C as fitting parameters. By plotting the fitted width C against time, see figure 4(d), we obtain from the slopes a diffusion coefficient of $D_L = 4.9 \times 10^{-13}$ m^2 s^{-1} for the liquid (L) phase. The viscosity of the liquid phase at statepoint III is $\eta_L = 21.5$ mPa s as measured with a Anton Paar Physica MCR300 rheometer. Assuming Stokes–Einstein behaviour leads to $D_L = k_B T/6\pi\eta_L R_c = 4.0 \times 10^{-13}$ m^2 s^{-1}, in good agreement with the results of the real-space technique. The diffusion coefficient of the gas phase can be measured in a similar way, but since the diffusion is much faster, it is more difficult to measure. In figure 4(d) the top two lines correspond to the measured widths for the gas (G) phase followed over a shorter time period. The linear fits give $D_G = 1.9 \times 10^{-12}$ m^2 s^{-1}, i.e. 3.7 times faster than diffusion in the liquid phase, whereas the viscosity is only 2.6 times smaller ($\eta_G = 8$ mPa s) and the deviation from Stokes–Einstein behaviour is thus larger. The liquid phase mostly consists of colloids, and experimentally it is often seen that in monodisperse colloidal sphere suspensions Stokes–Einstein behaviour for translational diffusion holds [41–43]. However, the gas phase has a high polymer concentration and there is much discussion about which cases Stokes–Einstein behaviour applies for diffusion in a polymer network (see for recent experiments for example [44, 45] in which interpretations are made in terms of the dynamics of the polymer networks, which lies outside the focus of the present work). From the diffusion coefficients we see that the colloids have diffused over $10\sigma_c$ in less than a second both in the gas as well

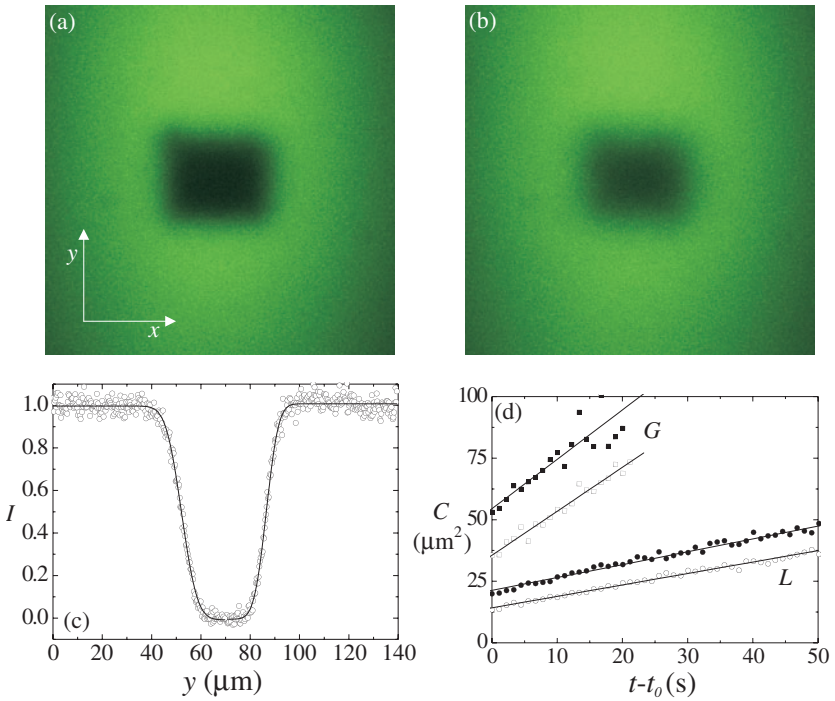

Figure 4. ((a), (b)) CSLM images ($140 \times 140\ \mu m^2$) of bleached cubes in the liquid phase at $t = 0$ s (a) and $t = 28$ s (b) for statepoint III (please note that the dynamics in statepoint I are very comparable). In (c) the intensity profiles along y of the image in (a) are shown. The curve is a fit to (9). In (d) the square root of the width of the profile is plotted as a function of time (minus the time t_0 between bleaching and the first recorded image) both for the liquid (circles) and the gas phase (squares) and for the top (filled symbols) and bottom (open symbols) sides. The full line is a linear fit. The slopes of these lines correspond to the diffusion coefficients in the liquid and gas phases. The CSLM scans pixel per pixel from left to right and top to bottom, which takes quite some time when bleaching the cube. This explains the offset for the two lines in the same phase, whereas the difference between liquid and gas is a direct consequence of the difference in diffusion coefficients ($D_L < D_G$).

as in the liquid phase. Since the time between sample homogenization and first observation is about 4 s, this explains why the interfaces are already sharp in the first recorded images.

4. Single wall behaviour

In figure 5(a) the gas–liquid interface close to a hard wall is shown. Although the interface looks very flat close to the wall in figure 1(a), the colloidal liquid phase clearly favours the wall. This was already seen by us in a silica-poly(dimethylsiloxane) mixture in cyclohexane [12] and later also confirmed by Wijting *et al* [46, 47]. The qualitative understanding of this phenomenon becomes apparent by considering all the depletion zones in play. The overlap at contact between the depletion zone of a colloidal particle and a wall is larger than the overlap between the depletion zones of two touching colloids. Thus, the colloidal rich phase, the liquid, favours the wall.

The shape of the meniscus is described by the interplay between hydrostatic and Laplace pressure, and close to the wall also the disjoining pressure plays a role. Here, we ignore this

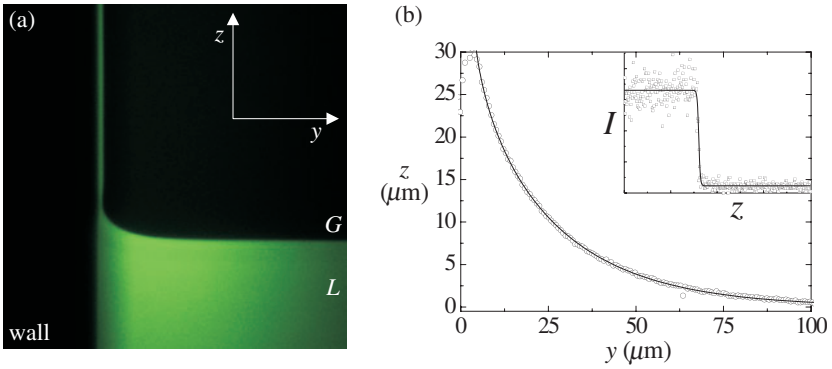

Figure 5. (a) CSLM image ($350 \times 350\ \mu m^2$) of the interface profile near a flat wall of statepoint II. Note that statepoint I has a comparable l_{cap}. (b) The interface from (a) (symbols) fitted to (11) (full curve). The inset shows the intensity along a single column in (a) described by a hyperbolic tangent function.

last term and by equating pressures we obtain the following differential equation

$$\Delta\rho g z = \gamma / R(z) \tag{10}$$

for the profile at a flat wall with $R(z)$ the radius of curvature at height z above the interface. The analytic solution for this problem is given in terms of $y(z)$, with y the distance to the wall, and is [48]

$$\frac{y}{l_{cap}} = \left[\operatorname{arccosh}\left(\frac{2l_{cap}}{z}\right) - \operatorname{arccosh}\left(\frac{2l_{cap}}{h}\right) + \left(4 - \frac{h^2}{l_{cap}^2}\right)^{\frac{1}{2}} - \left(4 - \frac{z^2}{l_{cap}^2}\right)^{\frac{1}{2}} \right], \tag{11}$$

with the capillary rise $h \equiv z(0)$. The shape of the profile only depends on l_{cap}, which thus can be found by fitting only a part of the profile. By extrapolating the profile to the wall one also obtains h and by the relation

$$h^2 = 2l_{cap}^2(1 - \sin\theta), \tag{12}$$

the contact angle can be measured. From figure 5(a) the interface can be accurately located, for example by fitting the intensity along a column in the z direction to a hyperbolic tangent function, which is shown as an inset in figure 5(b). The open circles in figure 5(b) are obtained with this method and denote the interface. The position of the wall can be determined using a similar method. Then we can either fit this profile directly to (11) with l_{cap} and h as fitting parameters or as in our previous work on wetting [12] define h (for example as $\sqrt{2}l_{cap}$) and then fit to (11) with l_{cap} and the position of the wall (a constant in the rhs of (11)) as fitting parameters. We here followed the second option and by comparing the fitted position with the actual position of the wall it is possible to obtain the actual h and hence the contact angle. Here we find $l_{cap} = 24\ \mu$m and $\theta = 0°$. As becomes apparent from the fit, (11) describes the experimental data points very well, implying that the macroscopic description of the interface still holds.

In [12] it was already noted that the apparent contact angle changes drastically close to the wall. For example, for $l_{cap} = 24\ \mu$m the apparent contact angle already becomes 16° only 0.7 μm away from the wall. This illustrates the necessity of using a fit-function in order to obtain the contact angle. With the present technique we succeed in measuring the contact angle accurately and without ambiguity.

In the present case, there is complete wetting, which also reveals itself by the liquid (wetting) layer seen at the wall. Remarkably, the layer has a thickness of about 2 μm and does not get considerably thinner higher up in the sample. Although this seems to be a non-equilibrium effect, no indications of convection were found, which was checked by bleaching experiments. We find that all our samples show complete wetting, which is in contrast with the predictions of Brader *et al* [16] (see also the very recent extension by Wessels *et al* [49]) and Dijkstra and van Roij [50], who used theory and simulations, respectively, and calculated a wetting transition reasonably close to the critical point. However, in their calculations the polymer was described as an ideal polymer, whereas in experiment the polymers are far from ideal. This has large effects on the bulk phase behaviour—several theories are present that correct for this [51–58]—and likewise for the wetting properties. Recently, we calculated the wetting transition within a Cahn model [59] for mixtures of colloids and excluded volume interacting polymers, which gives an improved description of the bulk phase behaviour and a reasonable agreement between predicted and measured interfacial tension. Moreover, it predicts a wetting transition far away from the critical point, even to above the triple point. This implies that the experimental observation of the transition becomes at least very difficult. In [46, 47] a wetting transition was claimed to be found, although the subtleties of the interfacial profile in reference to the contact angle—as explained above—were not fully realized.

5. Capillary condensation

We here follow the macroscopic derivation of Evans for the Kelvin equation of a two-component system [60, 61], which predicts the formation of a liquid condensate from an undersatured gas in a capillary slit. For two plates with area A and at a large separation l, as sketched in figure 6(a), the grand canonical potential Ω can approximately be written as the sum of bulk and surface contributions

$$\Omega_{\mathrm{G}} \approx -p_{\mathrm{G}} A l + 2\gamma_{\mathrm{wG}} A, \tag{13}$$

for gas (G) phase in the slit and

$$\Omega_{\mathrm{L}} \approx -p_{\mathrm{L}}^{+} A l + 2\gamma_{\mathrm{wL}} A, \tag{14}$$

for liquid (L) phase in the slit. Here, p_{G} and p_{L}^{+} are the pressures of the gas and liquid phases at a colloid chemical potential μ_{c} just below the bulk coexistence colloid chemical potential $\mu_{\mathrm{c}}^{\mathrm{coex}}$, and the bulk liquid phase is thus metastable (denoted by the +). The wall–gas and wall–liquid surface tensions are denoted by γ_{wG} and γ_{wL} and are connected via the Young–Laplace equation $\gamma_{\mathrm{wG}} = \gamma_{\mathrm{wL}} + \gamma_{\mathrm{GL}} \cos\theta$ with γ_{GL} the gas–liquid interfacial tension. Coexistence occurs if $\Omega_{\mathrm{G}} = \Omega_{\mathrm{L}}$ [60, 61] and using the Young–Laplace equation one obtains

$$p_{\mathrm{G}} - p_{\mathrm{L}}^{+} = 2\gamma_{\mathrm{GL}} \cos\theta / l. \tag{15}$$

By expanding the pressures around the coexistence pressure in both μ_{c} and μ_{p} (the polymer chemical potential) and using the Gibbs–Duhem relation $\Delta\mu_{\mathrm{p}} = -\Delta\mu_{\mathrm{c}}\, n_{\mathrm{c}}^{\mathrm{G}}/n_{\mathrm{p}}^{\mathrm{G}}$ with $\Delta\mu_x \equiv \mu_x^{\mathrm{coex}} - \mu_x$ and n_x^{G} the colloid or polymer number density in the gas phase (with x either p or c), we can write (15) as

$$\left(n_{\mathrm{c}}^{\mathrm{L}} - n_{\mathrm{c}}^{\mathrm{G}} \frac{n_{\mathrm{p}}^{\mathrm{L}}}{n_{\mathrm{p}}^{\mathrm{G}}} \right) \Delta\mu_{\mathrm{c}} = 2\gamma_{\mathrm{GL}} \cos\theta / l. \tag{16}$$

A condensate forms at a plate–plate separation l of twice the Kelvin length l_{K} (assuming $\cos\theta = 1$ as in the experiment), which is given as

$$l_{\mathrm{K}} = \frac{\gamma_{\mathrm{GL}}}{(n_{\mathrm{c}}^{\mathrm{L}} - n_{\mathrm{c}}^{\mathrm{G}}(n_{\mathrm{p}}^{\mathrm{L}}/n_{\mathrm{p}}^{\mathrm{G}}))\Delta\mu_{\mathrm{c}}}. \tag{17}$$

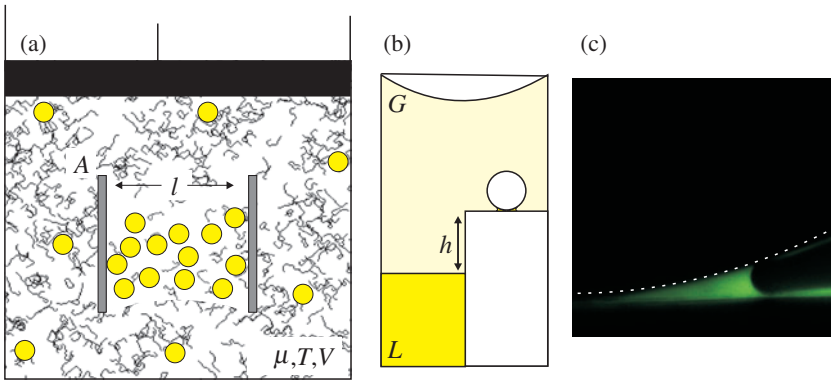

Figure 6. (a) Thermodynamic scheme for capillary condensation. (b) Schematic setup of the experiment. (c) CSLM image 175×175 (μm^2) showing the suction of liquid phase into the wedge at statepoint I. The dashed curve follows the contour of the glass sphere.

Without the factor $n_{\rm p}^{\rm L}/n_{\rm p}^{\rm G}$ equations (16) and (17) are equivalent to the one-component Kelvin equation (4). This factor approaches one close to the critical point and far away $n_{\rm c}^{\rm G}$ is small, so the difference between the one- and two-component Kelvin equation is very small. Using free volume theory [21] to calculate the phase behaviour of an ideal polymer–colloid mixture and a squared gradient theory to calculate the interfacial tension [18], it can be shown that the Kelvin length becomes of the order of tens of $\sigma_{\rm c}$ (i.e. micrometres in the present case) far away from the critical point and for small undersaturation $\Delta\mu_{\rm c} \sim 0.05\, k_{\rm B}T$. In [62] Schmidt *et al* calculate the phase behaviour of colloid–polymer mixtures between two walls using density functional theory and performing computer simulations. They find quit good agreement with the Kelvin equation, except close to the critical point.

Several possibilities exist to bring a colloid–polymer mixture slightly off-coexistence. In the present experiment we made use of gravity; see figure 6(b). At a distance h above the flat interface the intrinsic chemical potential $\mu_{\rm c}^{\rm i}$ for a colloid becomes $\mu_{\rm c}^{\rm i} = \mu_{\rm c}^{\rm coex} - m^* g h$. For the colloids in the present study with a density of 1.17 g ml^{-1} the gravitational length $l_{\rm g} = k_{\rm B}T/m^* g$ is $\sim$2.4 cm in the solvent decalin. At a distance of 0.5 cm above the colloidal gas–liquid interface, the system is off-coexistence by an amount $\Delta\mu_{\rm c} = 0.21\, k_{\rm B}T$. We ignore the effect of gravity on the polymer, since the polymer's buoyant mass is negligible. After phase separation had completed a glass sphere was dropped at the glass pedestal. The imaging technique works nicely and liquid phase clearly is present in the wedge, see figure 6(c), but the observed Kelvin length is of the order of 10 μm. From the capillary length measurements in section 4 one can estimate the interfacial tension to be at most 1 μN m^{-1} (which in principle follows from (3) if the gas–liquid density difference is known) and the Kelvin length then becomes less than a micrometre (17). Of course the thick wetting layers modify the Kelvin equation (16), and not necessarily in a straightforward manner—by simply setting the gap l in (16) as $l - 2t$ with t the thickness of the wetting layers—as was first recognized by Derjaguin [63]. Experimentally it appears as if liquid material is sucked into the capillary wedge due to capillary action; see figure 6(c). The discrepancy between observed and expected Kelvin length most probably indicates that the system did not yet reach complete equilibrium. It is difficult to estimate the time needed to reach complete equilibrium.

6. Conclusion

We have shown the possibilities and advantages of studying fluid–fluid demixing colloid–polymer mixtures with confocal scanning laser microscopy. The low capillary velocity allows

for a detailed study of demixing kinetics and morphology. The late stages of spinodal decomposition can be clearly followed and by Fourier transforming the CSLM images basically similar information as from light scattering experiments can be obtained. The coarsening rate of the characteristic length in the system can be understood in terms of the capillary velocity. At roughly three times the capillary length the spinodal structure collapsed, and phase separation occurred via gravity driven flow until a sharp interface formed. It is then possible to measure the diffusion coefficients by performing real space fluorescence recovery after photo-bleaching experiments. The measured colloid diffusion coefficient in the liquid phase is slightly larger than predicted from Stokes–Einstein behaviour, whereas in the gas phase it is much larger. Note that with the present technique it is also possible to measure diffusion close to walls or across interfaces. Already in a few seconds the colloids have diffused over many times their own diameter, which explains why in our experiments the first recorded images of spinodal decomposition have sharp interfaces.

The macroscopic colloidal gas–liquid interface near a flat wall is accurately described by the interplay between gravity and interfacial tension. With the present technique it is possible to measure the contact angle very accurately, and all samples show complete wetting. Finally, the potential of the technique is illustrated by the precise imaging of the colloid–polymer mixture between two walls. Analysing this effect in terms of capillary condensation shows that the relevant lengths are unexpectedly large, which possibly stands in close connection with the observed thick wetting layers. Several explanations could explain this observation: the disjoining pressure has an unexpected character, a subtle fractionation effect [64], in which the average colloid size in the gas phase is smaller than in the liquid phase, keeps the system closer to bulk coexistence even high up in the gas phase, or the system did not yet reach complete equilibrium. The origin for this observation is still to be investigated.

Acknowledgments

It is our pleasure to thank Roel Dullens for particle synthesis, Kees Rietveld for creating experimental setups, and our glass department for fabricating many ingenious glass cuvettes. Furthermore, we thank Susan Kersjes for pioneering experiments and Matthias Schmidt, Paul Wessels, Willem Kegel, Nikoleta Simeonova, Andrei Petukhov, Jan Dhont, Bob Evans and Roel Dullens for many fruitful discussions. This work was supported by the Stichting voor Fundamenteel Onderzoek der Materie (Foundation for Fundamental Research on Matter), which is part of the Nederlandse Organisatie voor Wetenschappelijk Onderzoek (Netherlands Organisation for Advancement of Research).

References

[1] Poon W 2002 *J. Phys.: Condens. Matter* **14** R589
[2] Hoogenboom J P 2002 Colloidal epitaxy, a real-space analysis *PhD Thesis* Utrecht University
[3] van Blaaderen A 1995 *Science* **270** 1177
[4] Asakura S and Oosawa F 1954 *J. Chem. Phys.* **22** 1255
[5] Asakura S and Oosawa F 1958 *J. Polym. Sci.* **33** 183
[6] Vrij A 1976 *Pure Appl. Chem.* **48** 471
[7] Wensink H H and Lekkerkerker H N W 2004 *Europhys. Lett.* **66** 125
[8] Schmidt M, Dijkstra M and Hansen J P 2004 *Proc. CODEF Conf.*; *J. Phys.: Condens. Matter* **16** S4185
[9] de Hoog E H A and Lekkerkerker H N W 1999 *J. Phys. Chem.* B **103** 5274
[10] Chen B H, Payandeh B and Robert M 2000 *Phys. Rev.* E **62** 2369
[11] de Hoog E H A and Lekkerkerker H N W 2001 *J. Phys. Chem.* B **105** 11636
[12] Aarts D G A L, van der Wiel J H and Lekkerkerker H N W 2003 *J. Phys.: Condens. Matter* **15** S245
[13] Aarts D G A L, Schmidt M and Lekkerkerker H N W 2004 *Science* **304** 847
[14] Vrij A 1997 *Physica* A **235** 120

[15] Brader J M and Evans R 2000 *Europhys. Lett.* **49** 678
[16] Brader J M, Evans R, Schmidt M and Löwen H 2002 *J. Phys.: Condens. Matter* **14** L1
[17] Moncho-Jorda A, Rotenberg B and Louis A A 2003 *J. Chem. Phys.* **119** 12667
[18] Aarts D G A L, Dullens R P A, Lekkerkerker H N W, Bonn D and van Roij R 2004 *J. Chem. Phys.* **120** 1973
[19] Bosma G, Pathmamanoharan C, de Hoog E H A, Kegel W K, van Blaaderen A and Lekkerkerker H N W 2002 *J. Colloid Interface Sci.* **245** 292
[20] Vincent B 1990 *Colloids Surf.* **50** 241
[21] Lekkerkerker H N W, Poon W C K, Pusey P N, Stroobants A and Warren P B 1992 *Europhys. Lett.* **20** 559
[22] Cahn J W 1961 *Acta Metall.* **9** 795
[23] Cahn J W 1965 *J. Chem. Phys.* **42** 93
[24] Dhont J K G 1996 *An Introduction to Dynamics of Colloids* (Amsterdam: Elsevier)
[25] Verhaegh N A M, van Duijneveldt J S, Dhont J K G and Lekkerkerker H N W 1996 *Physica* A **230** 409
[26] Bray A J 2000 Coarsening dynamics of nonequilibrium phase transitions *Soft and Fragile Matter: Nonequilibrium Dynamics, Metastability and Flow* ed M E Cates and M R Evans (Edinburgh: SUSSP Publications) (Bristol: Institute of Physics Publishing)
[27] Pagonabarraga I, Desplat J-C, Wagner A J and Cates M E 2001 *New J. Phys.* **3** 9.1
[28] Guenon P, Gastaud R, Perrot F and Beysens D 1987 *Physica* A **36** 4876
[29] Binder K and Stauffer D 1974 *Phys. Rev. Lett.* **33** 1006
[30] Chou Y C and Goldburg W L 1981 *Phys. Rev.* A **23** 858
[31] Tromp R H, Rennie A R and Jones R A L 1995 *Macromolecules* **28** 4129
[32] Lebowitz J L, Marro J and Kalos M H 1982 *Acta Metall.* **30** 297
[33] Furukawa H 1984 *Physica* A **123** 497
[34] Siggia E D 1979 *Phys. Rev.* A **20** 595
[35] Koenderink G H, Aarts D G A L, de Villeneuve V W A, Philipse A P, Tuinier R and Lekkerkerker H N W 2003 *Biomacromolecules* **4** 129
[36] Cates M E 2002 private communication
[37] Wysocki A and Löwen H 2004 *Phys. Rev.* E submitted
[38] Cahn J W and Hilliard J E 1958 *J. Chem. Phys.* **28** 258
[39] Cahn J W and Hilliard J E 1959 *J. Chem. Phys.* **31** 688
[40] Simeonova N and Kegel W K 2003 *Faraday Discuss.* **123** 27
[41] Kops-Werkhoven M M and Fijnaut H M 1982 *J. Chem. Phys.* **77** 2242
[42] van Blaaderen A, Peetermans J, Maret G and Dhont J K G 1992 *J. Chem. Phys.* **96** 4591
[43] Segrè P N, Meeker S P, Pusey P N and Poon W 1995 *Phys. Rev. Lett.* **75** 958
[44] Onyenemezu C N, Gold D, Roman R and Miller W G 1993 *Macromolecules* **26** 3833
[45] Koenderink G H, Sacanna S, Aarts D G A L and Philipse A P 2004 *Phys. Rev.* E **69** 021804
[46] Wijting W K, Besseling N A M and Stuart M A C 2003 *Phys. Rev. Lett.* **90** 196101
[47] Wijting W K, Besseling N A M and Stuart M A C 2003 *J. Phys. Chem.* B **107** 10565
[48] Batchelor G K 1967 *An Introduction to Fluid Dynamics* (Cambridge: Cambridge University Press)
[49] Wessels P P F, Schmidt M and Löwen H 2004 *Proc. CODEF Conf.*; *J. Phys.: Condens. Matter* **16** S4169
[50] Dijkstra M and van Roij R 2002 *Phys. Rev. Lett.* **89** 208303
[51] Fuchs M and Schweizer K S 2000 *Europhys. Lett.* **51** 621
[52] Aarts D G A L, Tuinier R and Lekkerkerker H N W 2002 *J. Phys.: Condens. Matter* **14** 7551
[53] Schmidt M and Fuchs M 2002 *J. Chem. Phys.* **117** 6308
[54] Bolhuis P G, Louis A A and Hansen J P 2002 *Phys. Rev. Lett.* **89** 128302
[55] Bolhuis P G, Louis A A and Meijer E J 2003 *Phys. Rev. Lett.* **90** 068304
[56] Schmidt M, Denton A R and Brader J M 2003 *J. Chem. Phys.* **118** 1541
[57] Chen Y-L, Schweizer K S and Fuchs M 2003 *J. Chem. Phys.* **118** 3880
[58] Paricaud P, Varga S and Jackson G 2003 *J. Chem. Phys.* **118** 8525
[59] Cahn J W 1977 *J. Chem. Phys.* **66** 3667
[60] Evans R and Marini Bettolo Marconi U 1987 *J. Chem. Phys.* **86** 7138
[61] Evans R 1990 *J. Phys.: Condens. Matter* **2** 8989
[62] Schmidt M, Fortini A and Dijkstra M 2003 *J. Phys.: Condens. Matter* **15** S3411
[63] Derjaguin B V 1940 *Acta Phys. Chem.* **12** 181
[64] Wessels P 2004 private communication